Math Geosci (2014) 46:241–260
DOI 10.1007/s11004-013-9505-y

SPECIAL ISSUE

Training Images from Process-Imitating Methods

An Application to the Lower Namoi Aquifer, Murray-Darling Basin, Australia

Alessandro Comunian · Sanjeev K. Jha · Beatrice M.S. Giambastiani · Gregoire Mariethoz · Bryce F.J. Kelly

Received: 15 January 2013 / Accepted: 4 November 2013 / Published online: 3 December 2013

Abstract The lack of a suitable training image is one of the main limitations of the application of multiple-point statistics (MPS) for the characterization of heterogeneity in real case studies. Process-imitating facies modeling techniques can potentially provide training images. However, the parameterization of these process-imitating techniques is not straightforward. Moreover, reproducing the resulting heterogeneous patterns with standard MPS can be challenging. Here the statistical properties of the paleoclimatic data set are used to select the best parameter sets for the process-imitating methods. The data set is composed of 278 lithological logs drilled in the lower Namoi catchment, New South Wales, Australia. A good understanding of the hydrogeological connectivity of this aquifer is needed to tackle groundwater management issues. The spatial variability of the facies within the lithological logs and calculated models is measured using fractal dimension, transition probability, and vertical facies proportion. To accommodate the vertical proportions trend of the data

A. Comunian (✉) · S.K. Jha · G. Mariethoz · B.F.J. Kelly
Connected Waters Initiative Research Centre, The University of New South Wales, Sydney, Australia
e-mail: alessandro.comunian@gmail.com

S.K. Jha
e-mail: s.jha@unsw.edu.au

B.F.J. Kelly
e-mail: bryce.kelly@unsw.edu.au

A. Comunian · S.K. Jha · G. Mariethoz · B.F.J. Kelly
National Centre for Groundwater Research and Training, Adelaide, Australia

B.M.S. Giambastiani
Physics and Earth Sciences Department, University of Ferrara, Ferrara, Italy
e-mail: gmbbrc@unife.it

G. Mariethoz
School of Civil and Environmental Engineering, University of New South Wales, Sydney, Australia
e-mail: gregoire.mariethoz@unsw.edu.au

set, four different training images are simulated. The grain size is simulated alongside the lithological codes and used as an auxiliary variable in the direct sampling implementation of MPS. In this way, one can obtain conditional MPS simulations that preserve the quality and the realism of the training images simulated with the process-imitating method. The main outcome of this study is the possibility of obtaining MPS simulations that respect the statistical properties observed in the real data set and honor the observed conditioning data, while preserving the complex heterogeneity generated by the process-imitating method. In addition, it is demonstrated that an equilibrium of good fit among all the statistical properties of the data set should be considered when selecting a suitable set of parameters for the process-imitating simulations.

Keywords Multiple-point statistics · Namoi river · FLUMY · Process-imitating · Direct-sampling · Conditioning data · Fluvial sedimentology

1 Introduction

Alluvial basins are important reservoirs of natural resources such as hydrocarbons and groundwater. To extract these resources efficiently, the complex architecture of the geological formations has to be characterized; this has proven to be a challenge for most interpolation techniques. Process-imitating methods (Koltermann and Gorelick 1996) can provide a credible representation of the sedimentary setting. However, such models are difficult to condition to local data such as boreholes or geophysical methods (Lopez 2003; Cojan et al. 2005; Michael et al. 2010). Multiple-points statistics (MPS, Guardiano and Srivastava 1993; Strebelle 2002) is a pixel-based technique which represents the observed lithological classes (lithofacies) at the right location. This method requires a training image (TI), which characterizes the desired facies distribution. One issue with MPS is that finding a suitable training image can be challenging, especially for three-dimensional cases (Hu and Chugunova 2008; Huysmans and Dassargues 2010; Le Coz et al. 2011). One way to obtain three-dimensional training images is from a combination of two-dimensional training images (Comunian et al. 2012); another is to simulate the three-dimensional training images with object-based techniques (Caers 2005; Maharaja 2008). However, when it comes to alluvial basins, process-imitating methods can provide three-dimensional training images in a more direct way. Note that here the term process-imitating is used in a broad sense and includes event-based methods (Pyrcz et al. 2012), process-based methods, and methods that combine stochastic and process-based methods (Lopez et al. 2001, 2009).

This paper investigates the use of a process-imitating method to provide training images for MPS simulations. Chugunova et al. (2007) and Chugunova (2008) presented one of the first applications of this approach. They used a synthetic case study and included an auxiliary variable to improve the reproduction of the continuous features of the training images. However, their technique requires defining the auxiliary variable over the complete simulation grid. Knowledge of the auxiliary variable over the problem domain is rarely available in real applications. Other authors included

a process-imitating method in their MPS simulation workflow (Michael et al. 2010). However, the process-imitating simulations are not used directly as training images for MPS, but to extract the information used to perform object-based simulations. Finally, the results of these object-based simulations are used as training images for multiple-point simulation.

Ultimately, there is a need to demonstrate the applicability of simulation workflows that include MPS in real case studies. Process-imitating methods can be used to simulate three-dimensional training images. However, reproducing the complex structures produced by process-imitating methods using the standard MPS simulation techniques is challenging, and is probably the main reason why such a workflow is not commonly used to simulate reservoirs or aquifers. One challenging aspect of inferring training images is that they need to encapsulate the geologists' knowledge about the sedimentary process relevant to the setting being modeled. Such knowledge is difficult to formalize, although it is critical for defining properties. For example, understanding the original paleoenvironment and tectonic history influences the appropriate selection of architectural features incorporated into the process-imitating model that will be used as the training image.

This paper presents an MPS simulation workflow that uses process-imitating derived training images (Fig. 1). In step 1, the process-imitating method and its parameters are selected using the statistical information inferred from the data set. The process-imitating method is then used to perform unconditional simulations. In step 2, the results of these simulations are used as training images to produce MPS conditional realizations. The grain size, one of the variables simulated by the process-imitating method, is used as an auxiliary variable in the MPS simulation to help preserve the realism of the sedimentary architecture in the simulated grid. The simulation workflow is tested using 278 lithological logs drilled in unconsolidated valley filling sedimentary sequence of the lower Namoi catchment, located in northern New South Wales, Australia (Fig. 2). The connectivity of this aquifer system is poorly understood, and better characterization of its heterogeneity is required to manage long term access to groundwater.

2 Methods

The site-specific information available for this study, described in Sect. 2.1, determines the criteria used to select the parameters for the process-imitating simulations and to validate the results of the simulations (Sect. 2.2). The simulation workflow consists of two main steps (Fig. 1): step 1, process-imitating simulation of the training images, and step 2, MPS simulation using the training images derived in step 1. Section 2.3 describes FLUMY (Cojan et al. 2005; Lopez et al. 2001, 2009; Lopez 2003), the process-imitating method used during step 1 to generate the training images. Here step 1 is tested on a synthetic case study (Sect. 2.4): first, a synthetic reservoir with FLUMY is simulated (Sect. 2.4.1); then, this reservoir is used as the reference data set in the sensitivity analysis and for validating the simulated training images (Sect. 2.4.2). The complete simulation workflow is tested on the lower Namoi case study data (Sect. 2.5). First (step 1, Fig. 1), the training images containing the

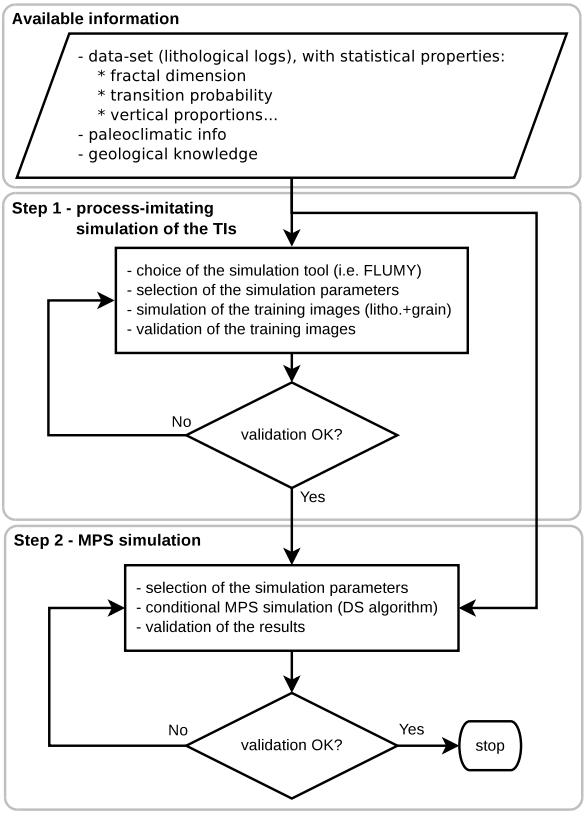

Fig. 1 Simulation workflow proposed in this study. Step 1, simulation of the training images with a process-imitating method; step 2, conditional MPS simulation using the training images simulated in step 1

main variable (the lithofacies) and the auxiliary variable (the grain size) are simulated with FLUMY. Then (step 2, Fig. 1), the training images simulated in step 1 are used to perform a MPS simulation using the direct sampling algorithm (DS), implemented in the DeeSse simulation software ("DS: Multiple-Point Simulation by Direct Sampling," Mariethoz et al. 2010).

2.1 The Lower Namoi Data Set

Our data set consists of 278 lithological logs drilled in an unconsolidated valley filling sedimentary sequence. Sediments at the base of the sequence were deposited in the mid Miocene by relatively high energy rivers, which deposited predominantly sands and gravels. Sediments in the upper 20 m were deposited in relatively low energy rivers, where floodplain deposits dominate over channel deposits. The logs were interpreted with a discretization step of 1 m and divided in two classes: sand+gravel rich sediments and clay+silt rich sediments. The logs cover an area of more than 9000 km^2, and the maximum topographic difference from the top of the logs is 82 m.

The horizontal correlation among the lithofacies is neglected because the distance between the logs is too large to allow the identification of correlated intervals, or a variogram structural element (the horizontal sand+gravel distribution is illustrated

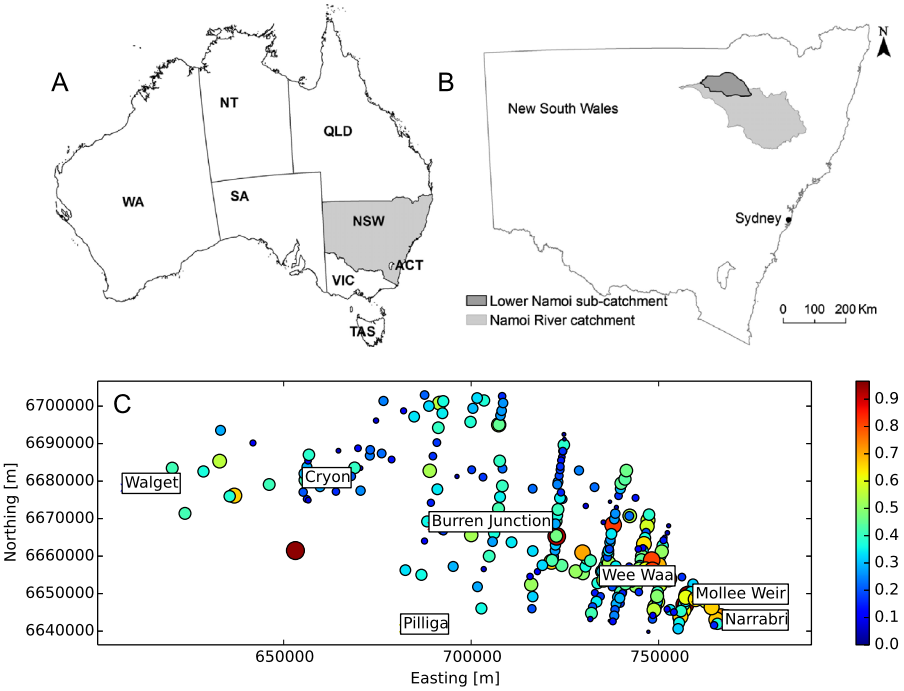

Fig. 2 The location of the lower Namoi sub-catchment and the sand+gravel proportions. (**C**) Distribution of the sand+gravel proportions. *Each point* represents the mean value of the proportion computed on a single log

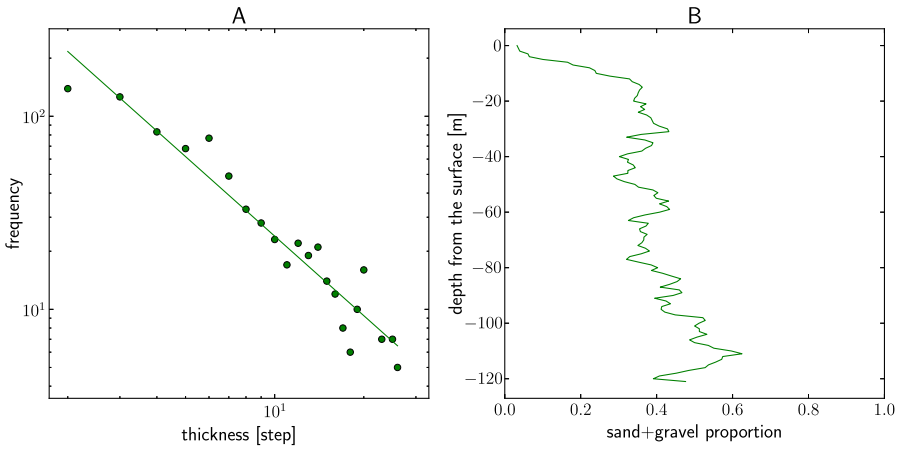

Fig. 3 (**A**) Fractal dimension; axes are logarithmic. (**B**) Vertical sand+gravel proportion curves

in Fig. 2C). Instead, the focus is on the vertical proportion curves (Fig. 3B) and on the information that can be extracted from them. While the statistical properties are inferred considering all 278 logs, the conditional simulations are performed in a vol-

ume defined by a square area with side 5 km centered on the town of Wee Waa. In this restricted area all the lateral non stationarities observed at the full scale of the lower Namoi catchment is neglected, and only one main sediment transport direction is considered.

2.2 Validation Criteria

Our data set provides sound statistical information mainly along the vertical direction. Therefore, most of the criteria used to check the consistency of our results are related to vertical statistical properties. Comparisons of the simulation grids are made using the data extracted from a number of vertical logs virtually drilled, at random locations, within the three-dimensional simulation domain. The vertical discretization step of the simulations (0.25 m for all the simulations presented here) is different from the discretization step of the data set. Therefore, the comparisons are always made at the same spatial scale, except for the fractal dimension, where only the discretization step is considered.

The following comparison criteria are considered: (i) Visual inspection: visually evaluate the simulation grids based on our geological knowledge of the site. (ii) Sand+gravel proportions: compare the sand+gravel vertical proportions computed on the logs with the proportions computed on the simulation grids. The proportions are computed considering the ground surface as the reference level. This is acceptable because the study area is quite flat. (iii) Fractal dimension: the sand+gravel layers identified in the logs drilled in the region have a fractal dimension D (Fig. 3A) that is compared with the fractal dimension of the simulation grids. To compute the fractal dimension, only vertical layers having a length of at least two discretization cells and a frequency of at least five occurrences is considered. The fractal dimension is the slope of the line fitted on the points having the vertical thickness of the sand+gravel layers t as abscissa and the frequency of the thickness f as ordinate (with logarithmic axes, Fig. 3A)

$$\log_{10}(f) = D \log_{10}(t) + c. \tag{1}$$

The choice of this criterion is inspired by the works of Bailey and Smith (2010). It is also akin to the concept of distribution of runs applied in a MPS context by Boisvert et al. (2007). (iv) Transition probabilities: the probability of transition from a given lithofacies to another at a given distance (Carle and Fogg 1996) is computed as follows: consider a categorical random field $Z(\mathbf{x})$ with values in $\{i = 0, 1\}$. The probability of observing the lithofacies (category) i at the location $\mathbf{x}_k$ is denoted $p_i(\mathbf{x}_k) = P[Z(\mathbf{x}_k = i)]$. With this notation, and from the definition of conditional probability, the transition probability of observing the lithofacies i at a location $\mathbf{x}_k$ and the lithofacies j at a location $\mathbf{x}_k + h$ can be defined as

$$tp_{i,j}(\mathbf{x}_k, \mathbf{x}_k + h) = \frac{P[Z(\mathbf{x}_k) = i \text{ and } Z(\mathbf{x}_k + h) = j]}{P[Z(\mathbf{x}_k) = i]}. \tag{2}$$

The transition probability curves of the logs and the simulation grids are compared. A root mean square (RMS) error of the differences in abscissa of the two curves is

computed and used as a numerical value for the comparisons. In this case indicator variograms could be used in place of the transition probability curves. (v) Dimensions of the sand+gravel bodies: from the geological knowledge of the site, the overall dimensions of the sand+gravel bodies are known in the first 10 m of depth only. Nevertheless, to have at least an approximated comparison criterion, the dimensions of the sand+gravel bodies in the simulation grids is computed. The vertical and the horizontal sizes of the sand+gravel bodies are computed with the following procedure: (1) the three-dimensional simulation grid is sliced in two-dimensional sections along planes perpendicular to the main direction of the channels; (2) for each slice, the sand+gravel bodies connected components are computed; (3) the dimensions of a rectangle that fully contains the sand+gravel bodies are computed; (4) the median value of the size of the rectangles is computed on all the sections. In the computation of the median size, the sand+gravel bodies with dimensions smaller than two discretization steps are ignored to account for the noise possibly generated during the simulations.

2.3 Process-Imitating Simulations

Our simulation workflow is valid for all the training images simulated with process-imitating methods. Here, the training images are simulated with FLUMY (Lopez et al. 2001, 2009; Lopez 2003), a combined stochastic and process-based method that is used here to obtain suitable proxies of process-imitating simulations. In FLUMY, the migration of the centerline of a channel is modeled using a modified version of the two-dimensional physical equations derived by Ikeda et al. (1981) and Sun et al. (1996, 2001). The channel has fixed width and height. At each iteration, a fullbank flood is simulated, together with the deposition of point bars, sand and mud plugs. The frequency of overbank floods can be periodic or stochastic, and the grain size and the thickness of the sediments deposited during these events are defined by an exponential function. The frequency of the levee breaches can be periodic or stochastic too, but it is also influenced by the flow velocity. The aggradation rate is controlled by defining a plane parallel to the flood plain, the so-called equilibrium profile.

2.4 Synthetic Case Study

To test step 1 of our methodology (Fig. 1), a synthetic model is generated with FLUMY using the default parameters. From this model, 278 virtual vertical logs are extracted to make our reference synthetic data set. Then, a sensitivity analysis is conducted on the channel dimensions and on the avulsion period, and the simulated training images are validated against the reference synthetic data set.

2.4.1 Simulation of the Reference Model

The reference model is simulated with FLUMY using the default parameters (Table 1). A simulation grid of size $200\times200\times200$ is used to keep the simulation time below few minutes, with cells of size (25, 25, 0.25 m) along x, y and z, respectively. This discretization is sufficient to represent a river like the Namoi, which presently

Table 1 Parameters used for the FLUMY simulations

	Parameter	Default value	Tested value
Channel	width [m]	100	from 50 to 250, step 5 to 10
	maximum depth [m]	4.35	from 2.7 to 6.5
Erodibility	coefficient [–]	2.0e–8	2.0e–8
Avulsion	type	Periodic	Periodic
	period [iterations]	1000	from 500 to 1500, step 100
Levee breach	type	Periodic	Periodic
	period [iterations]	600	600
	during overbank floods	no	no
	probability of CSI to CSII	0.5	0.5
	probability of CSII to CSIII	0.9	0.9
Aggradation	type	Periodic	Periodic
	period	100	100
	distribution	constant	constant
	thickness exponential decrease [m]	1000	1000
	grain size exponential decrease [m]	1000	1000
	width (multiple of the channel width)	6	6
Slope along x		0.001	0.001

has a width of the order of tens of meters, and to represent meanders, avulsions and other fluvial architectural features in their correct proportions over the domain.

FLUMY allows up to 10 different lithofacies to be simulated. However, the lithofacies logs were classified using only two categories. Therefore, all 10 FLUMY categories are assigned to one of the two categories used for the lithofacies log data. From the reference simulation grid 278 vertical logs are extracted, hereafter called virtual logs. These are used as the synthetic data set for comparisons performed during the sensitivity analysis.

2.4.2 Sensitivity Analysis and Training Images Validation

As a preliminary step to the sensitivity analysis, the variability of the validation criteria depending on the random seed used for the simulation is evaluated. In addition, this same variability is evaluated by changing the random location of the virtual logs extracted from the simulation grids.

The next step is the sensitivity analysis on the channel dimensions and the avulsion period. For this synthetic analysis, the real parameters of the process-imitating model are known. Using a random seed different from the one used for simulating the reference, 11 simulations are performed varying the channel width from 50 to 150 m with a step of 10 m (the channel depth is computed using the formula provided with the simulation software), and 11 simulations changing the avulsion period from 500 to 1500 iterations. Note that one iteration corresponds approximately to one year of sedimentary processes.

2.5 Lower Namoi Case Study

The simulation workflow is tested in its entirety (step 1 and step 2, Fig. 1) on the lower Namoi catchment data, which is scattered over more than 9000 km^2. Modeling such a large area with a high degree of realism is not feasible with commonly available computational resources. For example, suppose that one needs to represent a 50-m wide channel. The horizontal discretization should be at least 25 m, and to represent the sedimentary process along the vertical direction a discretization of at least 0.5 m is recommended in the FLUMY user's guide. With this discretization, the simulation grid for the lower Namoi catchment would require more than 10 billion nodes. Although grids of this size can be handled by the scientific community (Kollet et al. 2010), they require super computing resources. Here the computational grid of our study is restricted to a size that can be handled by a standard workstation. Therefore, the same grid size and discretization used in the synthetic case study are used here. The fractal dimension, transition probability, and the vertical proportions are computed using the lithofacies information from all 278 logs. For the conditional simulations, only logs within the bounds of the simulation grid centered on the town of Wee Waa are considered.

2.5.1 Simulation of the Training Images

FLUMY parameter values were initially set using insights from geological and paleoclimate knowledge of the lower Namoi catchment (Williams et al. 1989; Young et al. 2002). When the available information was insufficient to set a parameter value, the default FLUMY value was used. Default parameters are summarized in Table 1. For parameters that are uncertain, a sensitivity analysis is performed to compare the results of the simulations with the information available from the logs.

2.5.2 Sensitivity Analysis and Validation of the Training Images

The sensitivity analysis is performed by first varying the width and the depth of the channel: the width varies from 75 to 160 m with steps of 5 m; the depth is computed from the width at each step using the default FLUMY formula considering a parabolic cross section; the avulsion period is kept constant at 1000 iterations. In a second step, the simulations are performed with a constant channel dimension (width of 140 m and maximum depth of 5.5 m) and varying the frequency of the avulsion period from 100 to 1100 iterations, with steps of 100 iterations.

2.5.3 The Vertical Target Proportion

The vertical proportion curve has a non-stationarity trend (Fig. 3B). To replicate this with FLUMY, three simulation grids calculated with different parameter sets are stacked. From the results of the sensitivity analysis, the parameters yielding a good balance among the validation criteria considered are extracted, including the proportions for a given depth range. The following simulation layers are stacked: (1) first 30 m from the bottom, simulated with a channel width of 120 m and an avulsion period of 200 iterations; (2) second 50 m, simulated with a channel width of 120 m and

an avulsion period of 300 iterations; (3) finally, the top 42-m thick layer is simulated using a channel width of 100 m and an avulsion period of 400 iterations.

In the FLUMY simulations an equilibrium profile is not defined. When an equilibrium profile is not defined, in the uppermost simulation layers (that is, for the last iteration steps) the sedimentation process has not reached a mature state and the sand+gravel proportion decreases and approaches zero. This is suitable for the third uppermost layer because it allows us to reproduce the vertical sand+gravel proportion trend observed in the log data. Conversely, for the two other layers the upper part of the simulation grids is clipped to keep the sand+gravel proportion stable and close to the log data.

For reasons that are clarified in the next section, FLUMY is also used to simulate four separate training images. Two training images are simulated using the same parameters and dimensions of the first two layers described above. The other two training images are simulated with a thickness of 34 and 8 m, respectively, using parameters to target the mean sand+gravel vertical proportion observed in these two uppermost layers.

2.5.4 Multiple-Point Simulation

The conditional MPS simulation grids are calculated with the direct sampling algorithm (DS, Mariethoz et al. 2010), implemented in the DeeSse simulation software and described in brief. Consider a training image that represents the probabilistic model of a random variable Z, and a simulation grid where the values of Z are known at n locations only. These locations are at a lag distance $\{\mathbf{h}_1, \ldots, \mathbf{h}_n\}$ from a point $\mathbf{x}$ of the simulation grid where $Z(\mathbf{x})$ is to be simulated. To simulate this value with the DS, the training image is sampled at different locations $\mathbf{y}$ to look for a data event $\{Z(\mathbf{h}_1 + \mathbf{y}), \ldots, Z(\mathbf{h}_n + \mathbf{y})\}$ as close as possible to the data event $\{Z(\mathbf{h}_1 + \mathbf{x}), \ldots, Z(\mathbf{h}_n + \mathbf{x})\}$ contained in the simulation grid, according to a given distance measure and threshold. Once this data event is found, the corresponding value in the training image $Z(\mathbf{y})$ is assigned to the simulation grid at location $\mathbf{x}$. Then, the simulation proceeds sequentially until each simulation grid node has been assigned a value.

The DS approach can be generalized to make use of "vector images" (Hu and Chugunova 2008), which are training images that contain a vector random variable $\mathbf{Z}$ in place of Z. The sampling procedure described above is generalized by defining the appropriate distance measure (and the corresponding threshold) for each component of $\mathbf{Z}$. In this way it is possible to jointly simulate the components of $\mathbf{Z}$ on the simulation grid, or simulate one (or more) component(s) taking into account the conditioning provided by the remaining components.

FLUMY can simulate the grain size and the age of the formations alongside the lithofacies. Here the grain size is considered as an auxiliary variable to improve the quality of the DS simulation (Fig. 4E, F, G and H). Indeed, Chugunova et al. (2007) and Chugunova (2008) showed that without an auxiliary variable, reproducing the heterogeneity of the training images can be challenging. In FLUMY, the correlation between lithofacies and grain size can be complex, because it arises during different stages of the simulation process. For example, the grain size is defined in the migration process by the lithofacies deposited, while it is used differently in the exponential

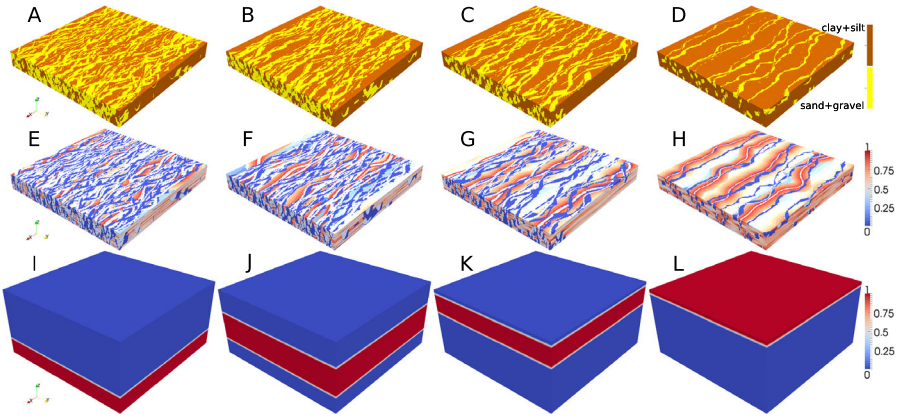

Fig. 4 (**A**), (**B**), (**C**) and (**D**) training images simulated with FLUMY. (**E**), (**F**), (**G**) and (**H**) normalized grain size. (**I**), (**J**), (**K**) and (**L**) probability maps of the training images. Both the normalized grain size and the probability maps are relative to the training image on the corresponding column. The vertical exaggeration for the training images and the grain size is 50×, while for the probability maps it is 20×

functions that define the sedimentation during the overbank floods. Nonetheless, this correlation is evident (Fig. 4) and helpful for guiding the MPS lithofacies simulation.

To deal with the non-stationarity along the vertical direction, the approach used here and implemented in the DeeSse software make use of multiple training images and a probability map defined on the simulation grid for each training image (Fig. 4). The probability maps are used during the DS simulation to select which training image to search for the required data event. For the selection of the best DS parameters, the guidelines proposed by Meerschman et al. (2013) and the results obtained on preliminary two-dimensional simulation tests are followed.

3 Results

3.1 Synthetic Case Study

The results of the sensitivity analysis performed by changing the dimensions of the channel and the avulsion period are summarized in Figs. 5 and 6, respectively. For each simulation the channel depth is varied together with the channel width. Therefore, in the following the terms channel width and channel dimensions are used synonymously. The fractal dimension is plotted for the logs virtually extracted from the simulation grids and reference model (Fig. 5A). The locations of the logs are changed for each comparison to observe the variability of the fractal dimension when the location of the virtually drilled logs is changed but the model remains the same. When the locations of the virtually-drilled logs in the reference model are changed, the fractal dimension varies from -0.7 to -0.54 (green continuous line for the mean value, green dashed lines for minimum and maximum, Fig. 5A). As expected, the variability is higher on the simulations performed changing the channel dimensions (red dashed line with triangles, Fig. 5A). When one looks at the fractal dimension

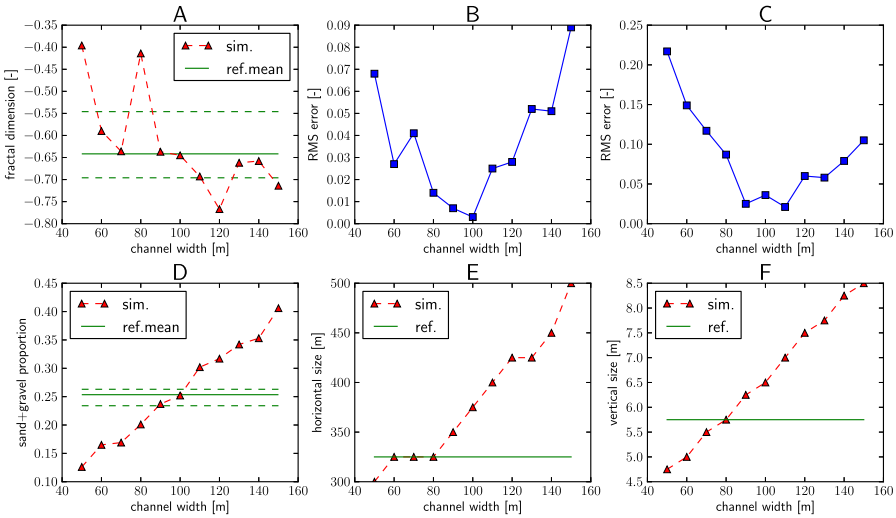

Fig. 5 Synthetic case study: sensitivity analysis on the channel dimensions. (**A**) Fractal dimension computed on the simulation grids and on the reference data set. (**B**) RMS error of the difference between the transition probability curves for the transitions from clay+silt to clay+silt. (**C**) Same as (**B**) but for the transitions from sand+gravel to sand+gravel. (**D**) Sand+gravel proportions. (**E**) Median horizontal size of the sand+gravel bodies. (**F**) Same as (**E**) but for the vertical size of the sand+gravel bodies. The reference model is simulated with a channel width of 100 m

curves of each individual simulation grid (not reported here), it is difficult to recognize the same clear fractal structure of the true data set (Fig. 3A). In this case, the fractal dimension does not help in the selection of the best parameter set. The RMS error of the differences between the transition probability curves for the logs drilled on the simulation grids and for the logs drilled on the reference model provides a good estimate of the parameters used to simulate the reference model. The line plots for the transitions from clay+silt to clay+silt (Fig. 5B) and for the transition sand+gravel to sand+gravel (Fig. 5C) have a minimum around the channel width 100 m. The variables considered here are binary variables, therefore the RMS errors are representative of the transitions from sand+gravel to clay+silt and from clay+silt to sand+gravel as well (Fig. 5B and C). The proportion of sand+gravel is plotted for each channel width tested (Fig. 5D). Variations induced by changing the location of the virtual logs in the reference model are small (sand+gravel proportions between 0.23 and 0.26, continuous green line mean value, dashed lines minimum and maximum, Fig. 5D). There is a positive linear trend between channel width and sand+gravel proportion (Fig. 5D). Parts E and F of the figure display the variation of the median of the horizontal and vertical size of the sand bodies. The sand+gravel bodies in the reference model have a median horizontal size of 325 m and a median vertical size of 5.75 m. There is a positive linear trend between channel width and these parameters computed for the simulation grids. The line plots computed for the simulation grids cross the reference model at a channel width value different from the reference one. Note that for the real case study, the figures cannot contain the line related to the reference because that information cannot be extracted from the lithological logs.

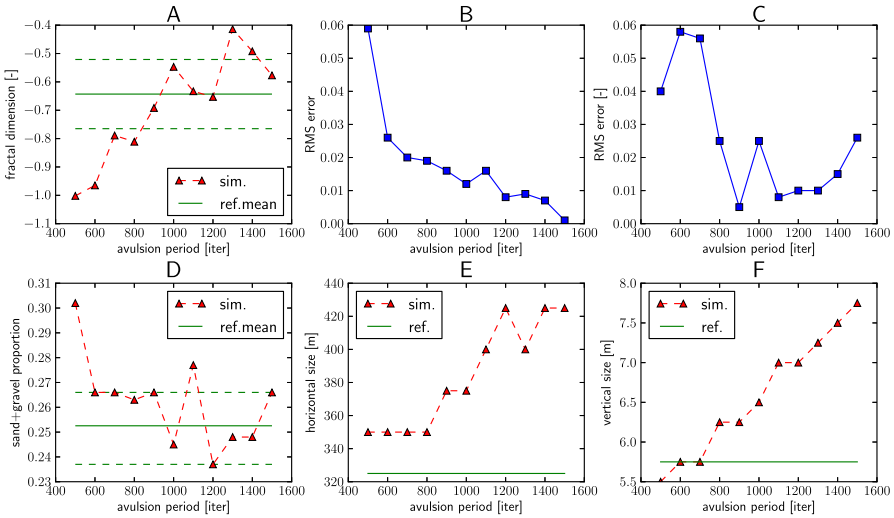

Fig. 6 Synthetic case study: sensitivity analysis on the avulsion period. See Fig. 5 and the text for more details. The reference model is simulated with an avulsion period of 1000 iterations

When the avulsion period is changed, the results obtained using the aforementioned criteria are different (Fig. 6). The fractal dimension is still unstable, but when computed on the simulation grids it has a clear positive linear trend, increasing when the avulsion period increases (Fig. 6A). A clearer trend can also be observed on the fractal dimension curves of each individual simulation grid (not reported here). It is difficult to infer the values of this parameter from the RMS error (Fig. 6B and C). For the transition from clay+silt to clay+silt there is no minimum, and for the transition from sand+gravel to sand+gravel the curve is unstable. Changing the avulsion period introduces a variation of the sand+gravel proportions smaller than changing the channel dimensions (23 to 30 % versus 12 to 40 %; note also the difference in the vertical scale between Figs. 5D and 6D). Therefore, the variations introduced by changing the location of the virtual logs in the reference model are comparable with the ones introduced changing the avulsion period. Consequently, the sand+gravel proportions are not useful for the determination of the reference parameter. For the vertical size of the sand+gravel bodies (Fig. 6F), it is difficult to infer from the intersections the value of the true parameter. The situation is even worse for the horizontal size, where for the avulsion periods considered there is no intersection of the two curves (Fig. 6E).

3.2 Lower Namoi Case Study

3.2.1 Sensitivity Analysis and Validation of the Training Images

The graphs that examine the sensitivity of the channel dimensions are displayed in Fig. 7. The fractal dimension is unstable and fluctuates far from the reference value of −1.4 (Fig. 7A). This behavior is reflected in the fractal dimension plots computed for each value of the channel dimension (not reported here), where it is not possible

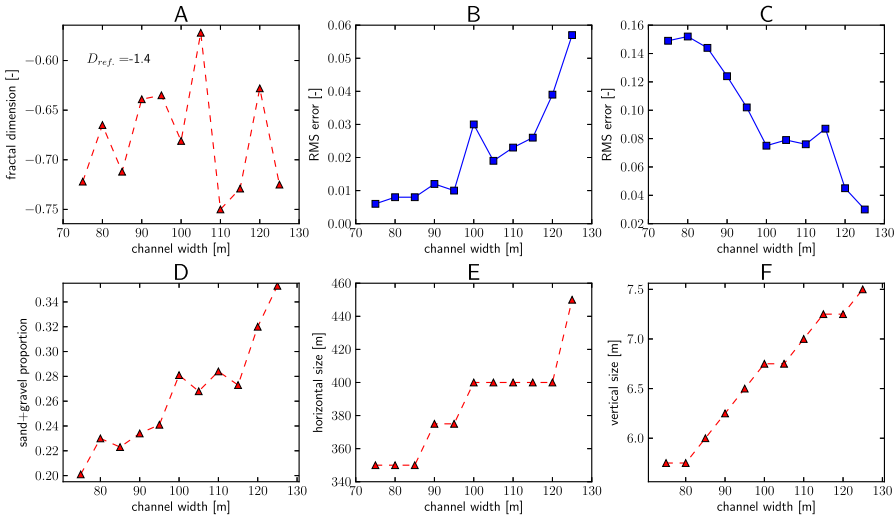

Fig. 7 Lower Namoi case study: sensitivity analysis on the channel dimensions. (**A**) Fractal dimension computed on the simulation grids. (**B**), (**C**) Same as Fig. 5B and C. (**D**) Sand+gravel proportions for the simulation grids. (**E**) Median horizontal size of the sand+gravel bodies of the simulation grids. (**F**) Same as (**E**) but for the vertical size of the sand+gravel bodies

to infer a clear fractal structure. The RMS errors of the transition probability curves are more stable than those for the fractal dimension curve (Fig. 7B and C). However, the inverse correlation between the two curves suggests that the best parameter can be selected as a compromise between the two RMS errors. The sand+gravel proportion (Fig. 7D) increases with the channel width. Here it is plotted only to provide an overview of the changes in sand+gravel proportions with the channel dimensions; the value of target proportion is not reported here because there is a strong non-stationarity in the data set, which is checked later by comparing the vertical proportion curves directly. The plots of the horizontal and vertical sizes of the sand+gravel bodies have a clear increasing trend (Fig. 7E and F). From this first part of the sensitivity analysis, considering in particular an equilibrium between the plots of the RMS error on the transition probability curves, the suitable value for the channel width is in the interval from 100 to 120 m.

Next the sensitivity analysis on the avulsion period (Fig. 8) is considered. In this case, the fractal dimension curve is more stable and presents a clear increasing trend when increasing the avulsion period (Fig. 8A). This stability can also be noticed in the fractal dimension curves plotted for a single value of avulsion period (not shown here). When the avulsion period is smaller than 1000 iterations (the default value used for the previous sensitivity analysis on the channel dimensions), these curves present a clear fractal structure. The RMS error on the transition probability curves from clay+silt to clay+silt has a clear decreasing trend when the avulsion period is increased (Fig. 8B), while the RMS error on the transition probability curves from sand+gravel to sand+gravel is unstable (Fig. 8C). When the sand+gravel proportions curves for the lower Namoi case study (Fig. 8D) and the synthetic case study (Fig. 6D) are compared, the former has a clearer decreasing trend. However, here

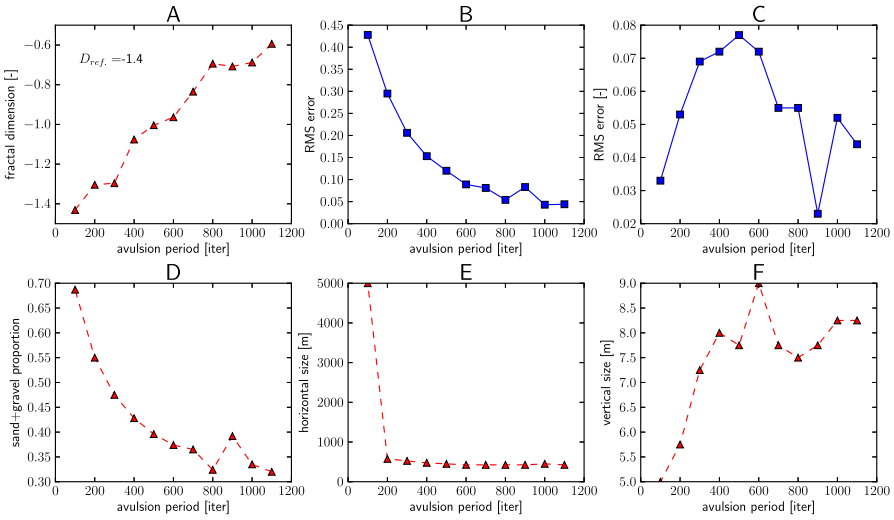

Fig. 8 Lower Namoi case study: sensitivity analysis on the avulsion period. See Fig. 7 and the text for a detailed description of the subplots

the avulsion period varies from 200 to 1100 iterations, while previously the range was 500 to 1500 iterations. Again, for the lower Namoi case study the proportions of the data set are not directly compared because they present a strong vertical non-stationarity. Except for an abrupt step for an avulsion period of 100 iterations, the horizontal size of the sand+gravel bodies decreases smoothly (Fig. 8E). The vertical size of the sand+gravel bodies increases and stabilizes around the value of 8 m for avulsion periods greater than 300 iterations. Taking into account the fractal dimension and the proportions, in the following the avulsion periods from 200 to 400 iterations are considered.

3.2.2 Matching the Vertical Target Proportions with FLUMY

A good fit to the trend is obtained by stacking different FLUMY simulations with different parameter sets (Fig. 9D). The parameter sets are selected using the suggestions provided by the previous sensitivity analysis. The fit on the fractal dimension is quite satisfactory (Fig. 9A). However, considering in more detail the trend of the fractal dimension for the simulation grid (triangles, Fig. 9A), it appears to contain more than one fractal dimension, and the linear fit could be divided in two parts. The fit of the transition probability curves for the transitions from clay+silt to clay+silt (Fig. 9B) and for the transitions from sand+gravel to sand+gravel (Fig. 9C) is a compromise. Indeed, an improvement of the fit for one transition often involves a deterioration of the fit for the other transitions (Fig. 7B and C). Therefore, the simulation parameters are selected to have a compromise between the fit of the two curves.

3.3 MPS Simulation

Comparing the DS simulation obtained using four different training images and a simulation obtained by stacking three different FLUMY simulation can give an idea

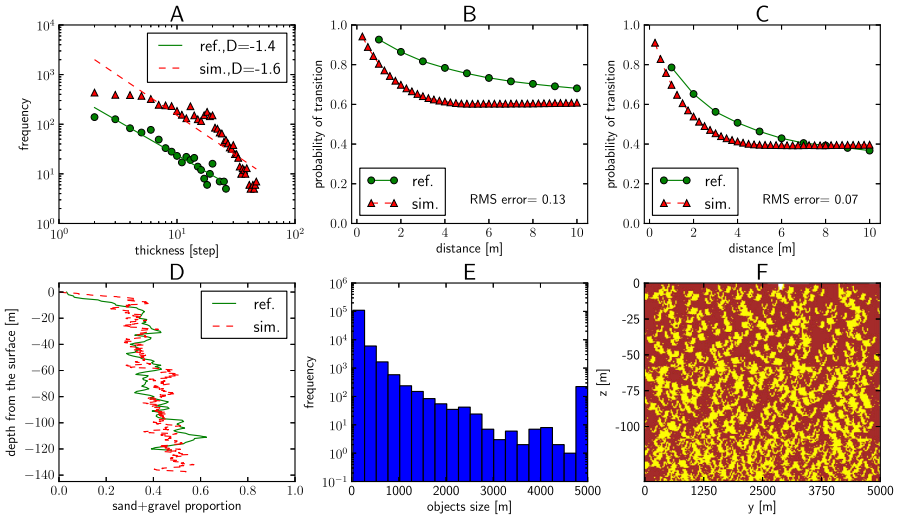

Fig. 9 Simulation performed stacking three FLUMY simulation grids with three different parameter sets. (**A**) Fractal dimension. (**B**) Transition probability curves computed for the transition from clay+silt to clay+silt. (**C**) Same as (**B**), but for the transitions from sand+gravel to sand+gravel. (**D**) Vertical sand+gravel proportion curves. (**E**) Histogram of the horizontal size of the sand+gravel bodies in the simulation grid. (**F**) Slice along the main direction of the channels at $x = 2500$ m; *yellow* represents sand+gravel and *brown* clay+silt; note the vertical exaggeration

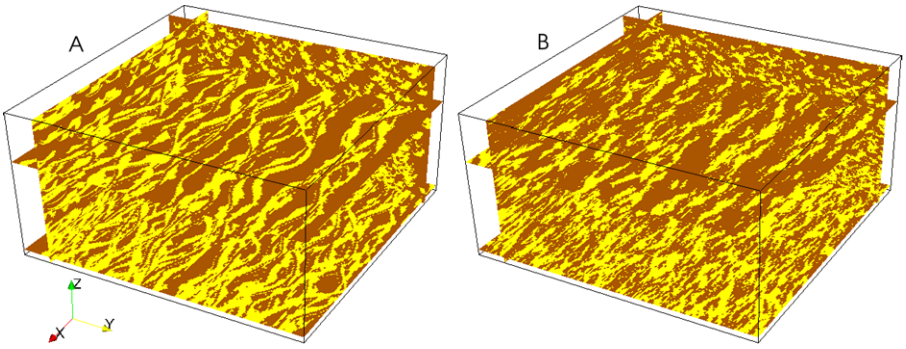

Fig. 10 (**A**) FLUMY simulation obtained by stacking three simulation grids with different parameters. (**B**) DS simulation obtained using four FLUMY training images (Fig. 4)

about the training reproduction, which in this case is not satisfactory (Fig. 10). The statistical properties of the DS simulation are compared with the reference data set (Fig. 11). The overall trends are similar to those of Fig. 9. Minor differences are in the fractal dimension curve, which is smoother (Fig. 11A), and also that all the sand+gravel bodies cut by a slice perpendicular to the flow direction are smaller than 4200 m (Fig. 11E).

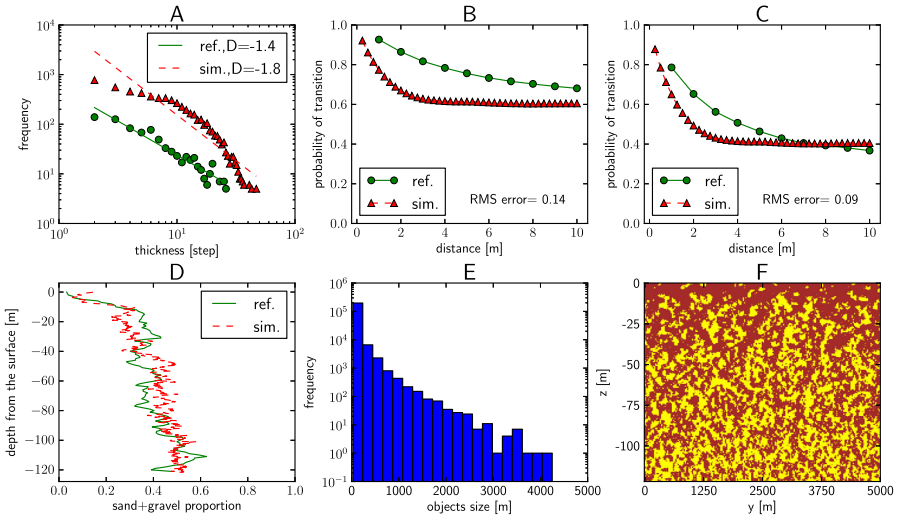

Fig. 11 Simulation performed using the DS with 4 training images and the grain size as an auxiliary variable (Fig. 4). See Fig. 9 for more details

4 Discussion

This study highlights a number of key issues when using process-imitating methods in conjunction with multiple-point statistics to characterize the facies heterogeneity of a valley filling sedimentary sequence. One issue in applying process-imitating methods is the selection of the right parameters to correctly represent the information contained in the data set. Here it is demonstrated that multiple criteria are needed to correctly compare the simulation grid with the reference data set. Indeed, a single criterion can be useful to suggest the best parameter in one situation, while the same criterion can be poor in other cases. This is illustrated in Figs. 7 and 8: for the sensitivity analysis on the channel dimensions the fractal dimension (Fig. 7A) is not a good criterion, while the RMS error on the transition probabilities (Fig. 7B and C) is useful; the opposite is true for the sensitivity of the avulsion period (Fig. 8). Even when the information provided by a criterion is not useful for precisely defining suitable simulation parameters, it can highlight the need to improve the parameterization. For example, an instability in the RMS error computed on the differences of the transition probability curves can be the symptom of an important difference between the reference and the simulation grids.

In our case, the fractal dimension of the simulation obtained by stacking many FLUMY simulation grids obtained with different parameter sets and that obtained by DS simulation is quite close to the reference (Figs. 9A and 11A). However, when considered closely, the curves appear to represent two different fractal scales. The change in slope around the value of 20 units probably corresponds to the maximum depth of the channel; for the FLUMY simulations, this parameter is set around the value of 5 m, which corresponds to the observed change in slope (red triangles, Fig. 9A). This change in slope is smoothed in the DS simulation grids (red triangles, Fig. 11A).

Overall, the change in slope of the curves representing the sand+gravel bodies' thicknesses versus their frequency indicates that too few thin and thick sand bodies are in the simulation grid.

The RMS error is a poor measure when the nature of the transition probability curves is different. However, even if the RMS values in these cases are not reliable (Fig. 8C), the curve trend suggests the need to improve the parameterization. The proportion curves are generally more stable indicators, even if a balance among all the parameters should always be considered. Considering the numerical values of the fractal dimension or of the RMS error on the transition probability without checking the individual curves (like the curves presented in Figs. 9A–C and 11A–C) can be misleading.

Even when using an auxiliary variable, with MPS it is difficult to reproduce in detail the lithofacies heterogeneity represented by the process-imitating simulation (Fig. 10). However, the exact reproduction of the training image is not our main goal and we consider it important to honor the statistical properties of the data set. These statistical properties are preserved by the MPS simulations and remain close to the properties of the reference model (Figs. 9 and 11).

5 Conclusions

This research demonstrates how process-imitating models can be constrained with statistical measures and used as the training image for conditional MPS simulations. The suitable process-imitating method and its parameters are inferred from the statistical properties of the data set. These properties include the fractal dimension, the transition probability curves and the proportion curves. The workflow has general validity and any other process-imitating method that generates a suitable representation of the depositional setting can be used. The MPS simulations performed with the DS algorithm only partially preserve the quality and the realism of the training images. Taking into account the grain size as a control variable improves the results. The training reproduction could be further improved by accounting for other characteristics of the training image, like connectivity indicators (Renard and Allard 2013). Other sources of information coming from the hydrological knowledge of a site, like for example hydrographs (Blakers et al. 2011), could be also included in the simulation workflow as well.

Another important aspect of this study is the sensitivity analysis performed to find the parameter sets suitable for reproducing the statistical features of the data set. A good balance between different validation criteria should be always considered. Future research should focus on an automated optimization of this process.

The non-stationarity in the vertical proportions is handled by dividing the simulation domain into different sub-domains where different training images are used. In this way a good fit with the observed lithofacies proportions is achieved. When tested on a real case study using the 278 vertical logs drilled in the lower Namoi catchment, northern New South Wales, Australia, the workflow yielded promising results. With the training images simulated in this work a problem at the scale of a small subdomain (25 km^2 area) of the lower Namoi aquifer is handled. The next challenge is

to extend the methodology to handle domains greater than this area and that include all the lateral non stationarity observed at the catchment scale.

Acknowledgements This work was supported by the National Centre for Groundwater Research and Training, Australia. The authors are grateful to F. Oriani, M.J. Pyrcz, the guest editor P. Renard, the editor in chief R. Dimitrakopoulos, and one anonymous reviewer for their constructive comments. They also acknowledge the University of Neuchâtel for providing the MPS simulation software DeeSse "DS: Multiple-Points Simulation by Direct Sampling".

References

Bailey R, Smith D (2010) Thematic set: scaling in stratigraphic data series: implications for practical stratigraphy. First Break. doi:10.3997/1365-2397.2010001

Blakers R, Kelly B, Anderssen B, Mariethoz G, Timms W (2011) 3D dendrogram analysis for mapping aquifer connectivity and flow model structure. In: MODFLOW and more 2011: integrated hydrologic modeling. Proceedings of the 10th international conference of the IGWMC, Colorado School of Mines, International Groundwater Modeling Center (IGWMC), Golden, Colorado, USA

Boisvert JB, Pyrcz MJ, Deutsch CV (2007) Multiple-point statistics for training image selection. Nat Resour Res 16(4):313–321. doi:10.1007/s11053-008-9058-9

Caers J (2005) Petroleum geostatistics. Society of Petroleum Engineers, Richardson

Carle S, Fogg G (1996) Transition probability-based indicator geostatistics. Math Geol 28:453–476. doi:10.1007/BF02083656

Chugunova T (2008) Contrainte des modèles génétiques de réservoirs par une approche de reconnaissance statistique de forme. PhD thesis, École des Mines, Paris

Chugunova T, Hu L, Lerat O (2007) Conditioning a process-based fluvial model using a non-stationary multiple-point statistics approach. In: EAGE petroleum geostatistics, extended abstract

Cojan I, Fouché O, Lopéz S, Rivoirard J (2005) Process-based reservoir modelling in the example of meandering channel. In: Leuangthong O, Deutsch C (eds) Geostatistics Banff 2004, Quantitative geology and geostatistics, vol 14. Springer, Dordrecht, pp 611–619. doi:10.1007/978-1-4020-3610-1_62

Comunian A, Renard P, Straubhaar J (2012) 3D multiple-point statistics simulation using 2D training images. Comput Geosci 40:49–65. doi:10.1016/j.cageo.2011.07.009

Guardiano FB, Srivastava RM (1993) Multivariate geostatistics: beyond bivariate moments. In: Soares A (ed) Geostatistics: Troia '92, vol 1. Kluwer, Dordrecht, pp 133–144

Hu LY, Chugunova T (2008) Multiple-point geostatistics for modeling subsurface heterogeneity: a comprehensive review. Water Resour Res 44(11):W11,413. doi:10.1029/2008WR006993

Huysmans M, Dassargues A (2010) Application of multiple-point geostatistics on modelling groundwater flow and transport in a cross-bedded aquifer. In: Atkinson PMM, Lloyd CDD (eds) GeoENV VII, geostatistics for environmental applications. Quantitative geology and geostatistics, vol 16. Springer, Dordrecht, pp 139–150

Ikeda S, Parker G, Sawai K (1981) Bend theory of river meanders. 1. Linear development. J Fluid Mech 112:363–377. doi:10.1017/S0022112081000451

Kollet SJ, Maxwell RM, Woodward CS, Smith S, Vanderborght J, Vereecken H, Simmer C (2010) Proof of concept of regional scale hydrologic simulations at hydrologic resolution utilizing massively parallel computer resources. Water Resour Res 46(4):W04,201. doi:10.1029/2009WR008730

Koltermann CE, Gorelick SM (1996) Heterogeneity in sedimentary deposits: a review of structure-imitating, process-imitating, and descriptive approaches. Water Resour Res 32(9):2617–2658. doi:10.1029/96WR00025

Le Coz M, Genthon P, Adler PM (2011) Multiple-point statistics for modeling facies heterogeneities in a porous medium: the Komadugu-Yobe alluvium, Lake Chad basin. Math Geosci 43:861–878. doi:10.1007/s11004-011-9353-6

Lopez (2003) Modélisation de réservoirs chenalisés méandriformes, approche génétique et stochastique. PhD thesis, École des Mines, Paris

Lopez S, Galli A, Cojan I (2001) Fluvial meandering channellized reservoirs: a stochastic and process based approach. In: IAMG annual meeting, Cancun, Mexico

Lopez S, Cojan I, Rivoirard J, Galli A (2009) Process-based stochastic modelling: meandering channelized reservoirs. Wiley/Blackwell, New York/Oxford, pp 139–144. doi:10.1002/9781444303131.ch5

Maharaja A (2008) Tigenerator: object-based training image generator. Comput Geosci 34(12):1753–1761
Mariethoz G, Renard P, Straubhaar J (2010) The direct sampling method to perform multiple-point geostatistical simulations. Water Resour Res 46(11):W11,536. doi:10.1029/2008WR007621
Meerschman E, Pirot G, Mariethoz G, Straubhaar J, Meirvenne MV, Renard P (2013) A practical guide to performing multiple-point statistical simulations with the direct sampling algorithm. Comput Geosci 52(0):307–324. doi:10.1016/j.cageo.2012.09.019
Michael HA, Li H, Boucher A, Sun T, Caers J, Gorelick SM (2010) Combining geologic-process models and geostatistics for conditional simulation of 3-d subsurface heterogeneity. Water Resour Res 46(5):W05,527. doi:10.1029/2009WR008414
Pyrcz MJ, McHargue T, Clark J, Sullivan M, Strebelle S (2012) Event-based geostatistical modeling: description and applications. In: Abrahamsen P, Hauge R, Kolbjørnsen O (eds) Geostatistics Oslo 2012. Quantitative geology and geostatistics, vol 17. Springer, Dordrecht, pp 27–38. http://dx.doi.org/10.1007/978-94-007-4153-9_3. doi:10.1007/978-94-007-4153-9_3
Renard P, Allard D (2013) Connectivity metrics for subsurface flow and transport. Adv Water Resour 51(0):168–196. http://www.sciencedirect.com/science/article/pii/S0309170811002223. 35th Year Anniversary Issue. doi:10.1016/j.advwatres.2011.12.001
Strebelle S (2002) Conditional simulation of complex geological structures using multiple-point statistics. Math Geol 34:1–21. doi:10.1023/A:1014009426274
Sun T, Meakin P, Jøssang T (2001) Meander migration and the lateral tilting of floodplains. Water Resour Res 37(5):1485–1502. doi:10.1029/2000WR900343
Sun T, Meakin P, Jossang T, Schwarz K (1996) A simulation model for meandering rivers. Water Resour Res 32(9):2937–2954. doi:10.1029/96WR00998
Williams N, Merrick RP, Ross J (1989) Natural and induced recharge in the lower Namoi valley, New South Wales. In: Sharma M (ed) Groundwater recharge. Proceedings of the symposium on groundwater recharge, 6–9 Luly, 1987. Balkema, Rotterdam, pp 239–253
Young RW, Young ARM, Price DM, Wray RAL (2002) Geomorphology of the Namoi alluvial plain, northwestern New South Wales. Aust J Earth Sci 49(3):509–523. doi:10.1046/j.1440-0952.2002.00934.x